Available online at www.sciencedirect.com
ScienceDirect
Polymer Degradation and Stability 93 (2008) 281–290
Polymer Degradation and Stability
www.elsevier.com/locate/polydegstab

'Tail' phenomenon and fatigue crack propagation of PC/ABS alloy

Qin-Zhi Fang, T.J. Wang*, H.M. Li

MOE Key Laboratory for Strength and Vibration, Department of Engineering Mechanics, Xi'an Jiaotong University, Xi'an 710049, China

Received 17 June 2007; received in revised form 4 September 2007; accepted 7 September 2007
Available online 12 November 2007

Abstract

The fatigue crack propagation (FCP) behavior of the alloy of polycarbonate (PC) and acrylonitrile–butadiene–styrene (PC/ABS) is experimentally investigated in this paper. An improved compliance method is employed to measure the fatigue crack length and optical and scanning electron microscopes (SEM) are used to observe the features of crack tip deformation *in situ*. 'Tail' phenomenon has been observed at the initial stage of fatigue for each specimen, which is regarded as a reflection of the transition process of accumulation of damage and plastic deformation during FCP. The law of FCP from low to high crack growth rate (10^{-6}–10^{-3} mm/cycle) is obtained and described with Paris law. Porous or dimple features govern the fatigue crack surfaces and coarse features have been seen on the crack surfaces with higher crack growth rate, while smooth features have been observed on the crack surfaces with lower crack growth rate. A stretched band appears when the crack growth transforms from lower to higher region of FCP rate.

Keywords: Fatigue; Crack propagation; Tail phenomenon; Polymer; PC/ABS alloy; Compliance method

1. Introduction

Fatigue failure is one of the main failure modes in engineering structures. Polymer is being widely used in some important engineering structures, such as the structures in aerospace, automobile, pressure vessels and pipes, etc. Therefore, investigation of the fatigue and fracture of polymer is important and extensive researches have been devoted to this field. Effects of loading parameters and microstructures on the fatigue crack growth of polymers have been carried out [1–7]. Lowe et al. [1] studied the microstructure, fracture and fatigue behavior of rubber modified CIBA GEIGY GY260 cured with piperidine. Bureau et al. [2,3] studied the fatigue crack propagation (FCP) of injection-moulded polystyrene (PS) and PS/high-density polyethylene (HDPE) blend at loading frequencies of 2 Hz and 20 Hz, in which the effect of blend composition, loading frequency and crack propagation direction were discussed. The effects of stress ratio and molecular weight on fatigue characteristics of polymers are also investigated [4,5]. It was shown that the square waveform ''off-load'' time had a great effect on the fatigue crack propagation of ethylene homopolymers and ethylene–hexene copolymers [6,7]. On the other hand, Pruitt and Bailey [8] studied the effects of manufacture process (such as compression molding or ram extrusion), sterilization, aging environment and notch orientation relative to the extrusion direction on the FCP of orthopedic grade ultra high molecular weight polyethylene (UHMWPE). Baker et al. [9] studied the effects of morphology, sterilization with or without accelerated aging and temperature on the FCP of medical grade UHMWPE under compression and tension fatigue loading conditions. Shah et al. [10] studied the correlation of FCP in polyethylene (PE) pipe with different specimen geometries. Also, the slow crack propagation in a real PE pipe was experimentally studied through fatigue test with compact tension (CT) specimens [11]. Parsons et al. [12] experimentally studied the damage zone ahead of the arrested crack in high and medium density polyethylenes (HDPE and MDPE). It was

* Corresponding author. Tel./fax: +86 29 82665168.
E-mail addresses: fangqz@mail.xjtu.edu.cn, wangtj@mail.xjtu.edu.cn (T.J. Wang).

0141-3910/$ - see front matter © 2007 Elsevier Ltd. All rights reserved.
doi:10.1016/j.polymdegradstab.2007.09.002

shown that the shape of the damage zone had great influence on the crack growth behavior of these materials.

Generally, cyclic loading can induce large number of tiny cracks near a defect, which leads to the reduction of fracture strain and to the brittleness of polymer [13–16]. Studies on the fatigue of rubber-toughened blends have shown that the presence of rubber particles in a brittle thermoplastic matrix generally leads to a reduction of resistance to fatigue crack initiation in unnotched specimens and to an improvement of resistance to fatigue crack propagation in pre-cracked specimens [2,3,8,13–18]. The surfaces of fatigue cracks are different for different crack growth rates. Discontinuous crack growth bands (DGBs) appear on the crack surfaces at low rates of fatigue crack growth associated with crazed material in the plastic zone, dimple structures appear on the fracture surfaces at moderate rates of fatigue crack growth, and striation structures are found on the fracture surfaces at high fatigue crack growth rates [12,17–23]. It is found that the rate of fatigue crack growth can either decrease or not change significantly with increasing loading frequency [2,3,8,14].

Investigations of the deformation and fracture of PC/ABS alloy are carried out as well [17,23–26]. A few works have been carried out on the fatigue of PC and PC/ABS alloy [17]. However, investigations of crack growth of polymer are mainly focused on the crack growth rate over 10^{-5} mm/cycle [2–5,9]. Fatigue crack growth rate below 10^{-5} mm/cycle is considered in the region of near threshold [5], but there are no sufficient studies carried out. Therefore, further study on fatigue behavior of polymer with lower crack growth rate is necessary.

The objective of this work is to experimentally investigate the FCP behavior of PC/ABS alloy within a large range of crack growth rate. An improved compliance method [27] is employed to measure the fatigue crack propagation. *In situ* optical and SEM observations are carried out to investigate the mechanisms of crack tip deformation and fatigue process. SEM observation is carried out to analyze the fracture surface. Some interesting features are obtained.

2. Experimental

2.1. Materials and specimens

The material considered here is PC/ABS alloy. The average molecular weight of base material PC is 26 000 g/mol. SWA compatibilizer is added to the blend of PC and ABS before injection. Composition of PC/ABS alloy is 66/30/4 PC/ABS/SWA, in which ABS has different pellet sizes mainly of 0.2–0.5 μm diameters. The injection temperature of the plates of PC/ABS alloy is 240–250 °C. The holding pressure is 60–80 MPa.

Compact tension (CT) specimens with thickness B of 2.8 mm, width W of 50 mm, notch depth of 15 mm and notch opening width of 2 mm are designed according to standard ASTM E-647, as shown in Fig. 1a. The specimens are carefully manufactured from PC/ABS plates with dimensions of 167 mm × 102 mm × 3 mm. Before fatigue testing, a small pre-crack of 1.5–2 mm at the notch tip for each specimen is manually introduced by slowly pushing a fresh razor blade into the specimen along with the direction of the notch. Generally, the pre-crack is cut several days before the fatigue test is performed, so that the possible residual stresses induced at the crack tip can be released some what before fatigue testing. After that, the initial crack length a_0, which is about 17 mm, is carefully measured with an optical microscope. Fig. 2 shows macro- and microviews of the crack tip cut with a fresh razor. It is found that no obvious plastic deformation is found at the crack tip.

To observe the micromechanisms of fatigue crack growth of polymer, single edge crack tension specimens are cut from the CT specimens, as depicted in Fig. 1b. Then, the single edge crack specimens with an initial fatigue crack of about 4 mm length are used for the *in situ* scanning electronic microscope (SEM) observation of fatigue mechanism during and after overloading.

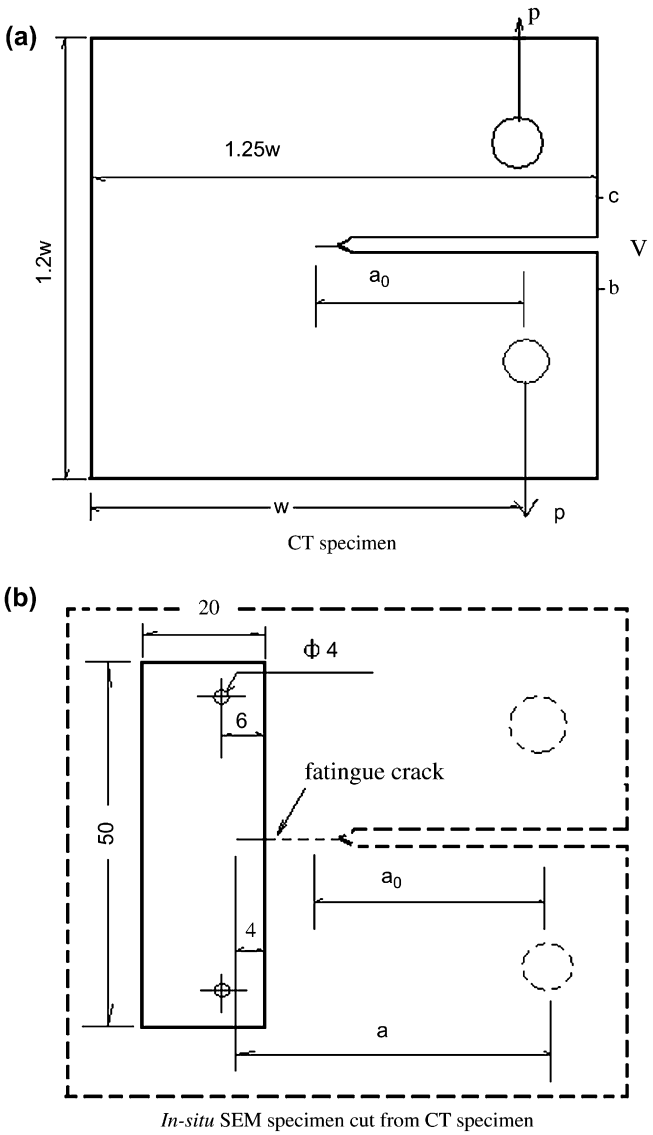

Fig. 1. Geometry and dimensions of the specimens with W being the width of the specimen, V the displacement measured by the displacement gage mounted on the specimen between b and c, P the fatigue load.

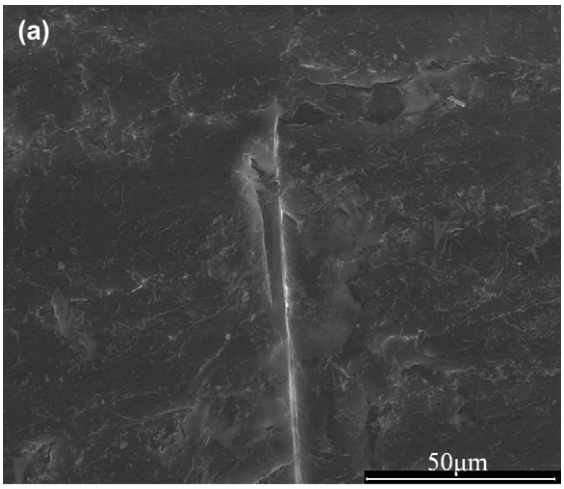

Fig. 2. Crack tip introduced by pushing a fresh razor blade slowly into the specimen.

2.2. Fatigue testing

Fatigue crack propagation experiments at room temperature (about 24 °C) in air are performed following standard procedures with a computer-controlled INSTRON-5848 machine. Sinusoidal waveform constant fatigue loading range (between P_{max} and P_{min}) at a frequency of 3 Hz and the minimum load P_{min} to the maximum P_{max} load ratio R (=P_{min} and P_{max}) of 0.1 is applied. Fatigue loads with different loading ranges (P_{max}−P_{min}) are imposed on the CT specimens during testing, so that FCP behavior over a large range of fatigue crack propagation rate (10^{-6} mm/cycle−10^{-3} mm/cycle) can be obtained. The variation of on-line crack mouth opening displacement V and load P data are collected every 300 cycles during the FCP tests, so that crack length can be obtained from compliance technique given in Section 2.4. The crack mouth opening displacement V is measured with a clip gage mounted on the CT specimen with a gage length of 10 mm, at points b and c, as shown in Fig. 1a. In addition, a traveling visual microscope is used to follow the crack propagation process, which can provide a calibration for the crack length obtained from compliance technique. The crack tip deformation too can be observed with the traveling visual microscope.

2.3. Micro- and macroscopic observations

SEM with fatigue loading device is used for the *in situ* observation of the crack tip deformation during fatigue loading by using small specimens as shown in Fig. 1b. The eccentric single edge cracked tension specimens are cut from the CT specimens that are fatigue cracked in the FCP test. In this way, an initial crack length of about 4 mm is obtained before the *in situ* SEM observation. The loading frequency and stress ratio are 0.08 Hz and $R = 0.1$, respectively, for the small *in situ* specimens. On the other hand, the fracture surfaces of other fatigue specimens are observed in SEM.

In all of the cases, an optical microscope is used to observe the crack tip deformation *in situ* as well as to measure the crack length manually.

2.4. Measurement and calculation of fatigue crack propagation

The fatigue crack length is measured by using an improved compliance method [27]. The load P vs. crack opening displacement V curve is obtained during fatigue loading. Fig. 3 shows one of the typical curves during the loading cycles. According to standard ASTM E-399, the following formula is used to calculate the dimensionless compliance $BE'\Delta V/\Delta P$ for CT specimen,

$$\frac{BE'\Delta V}{\Delta P} = \frac{19.75}{(1-a/W)^2}\left[0.5 + 0.129\left(\frac{a}{W}\right) + 1.385\left(\frac{a}{W}\right)^2 - 2.919\left(\frac{a}{W}\right)^3 + 1.842\left(\frac{a}{W}\right)^4\right] \quad (1)$$

where B is the thickness of the specimen, E' the elastic modulus of the material, a the crack length, W the width of the specimen, ΔV the increment of the crack opening displacement and ΔP the load increment. E' is equal to the Young's

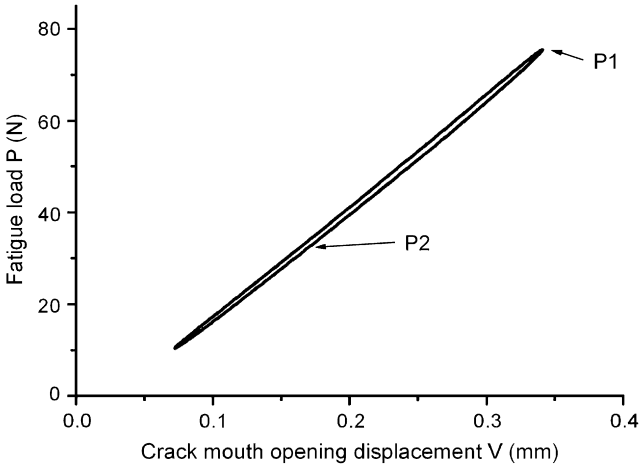

Fig. 3. Load−displacement curve.

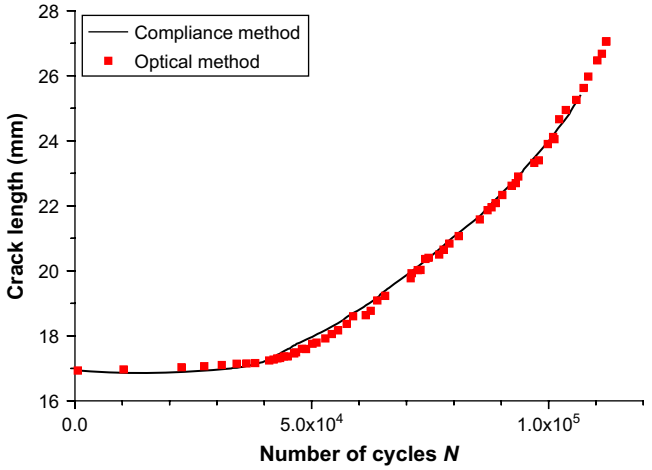

Fig. 4. Comparison of the a–N curves of a specimen measured from compliance and visual microscope methods.

modulus E in the case of plane stress field and equal to $E/(1-\nu^2)$ with ν being the Poisson's ratio in the case of plane strain field.

To eliminate the errors induced by various factors in fatigue experiments, such as the machine stiffness, the variations of specimen dimensions, the gage mounting error, etc. $\Delta V/\Delta P$ is replaced with $(C - C_0)$, in which C is the compliance calculated by best fitting with the data pairs (P, V) collected from the maximum load P_1 $(=P_{\max})$ to a lower load P_2 (about $1/3P_{\max}$) along the unloading line as shown in Fig. 3, and C_0 is a constant that could be used to adjust the value of compliance according to the measured value of compliance at certain known crack length. E' can be obtained according to the calibration of the crack length measured with optical method, which could be used to accommodate the viscous property of the polymer material.

To verify the precision of the crack length obtained from the above compliance method, an optical microscope is used to measure the crack length during fatigue test. The microscope could be moved in a three-dimensional traveling platform. Commercial software Image-Pro Plus 5.1 is employed to analyze the serial pictures taken during fatigue tests, from which the a–N curves of crack length a vs. fatigue cycle N can be obtained. Validity of the results obtained from the improved compliance method can be verified through the comparison of the a–N curves measured with optical microscope.

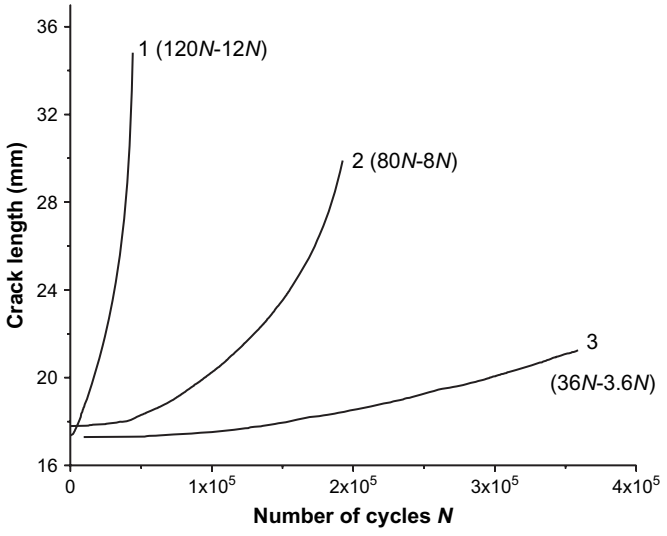

Fig. 5. a–N curves of PC/ABS alloy under different fatigue loadings. 1: $(P_{\max}, P_{\min}) = (120N, 12N)$, 2: $(P_{\max}, P_{\min}) = (80N, 8N)$ and 3: $(P_{\max}, P_{\min}) = (36N, 3.6N)$.

According to standard ASTM E-647, the range of stress intensity factor (SIF) ΔK can be calculated by using the measured data of a and N,

$$\Delta K = \frac{\Delta P_r}{B\sqrt{W}} \frac{2 + a/W}{(1 - a/W)^{3/2}} \left[0.866 + 4.64\left(\frac{a}{W}\right) - 13.32\left(\frac{a}{W}\right)^2 + 14.72\left(\frac{a}{W}\right)^3 - 5.6\left(\frac{a}{W}\right)^4\right] \quad (2)$$

and then the well-known Paris law,

$$\frac{da}{dN} = C(\Delta K)^m \quad (3)$$

can be employed to describe quantitatively the FCP rate relation, in which ΔP_r is the fatigue loading range, and C and m are material constants.

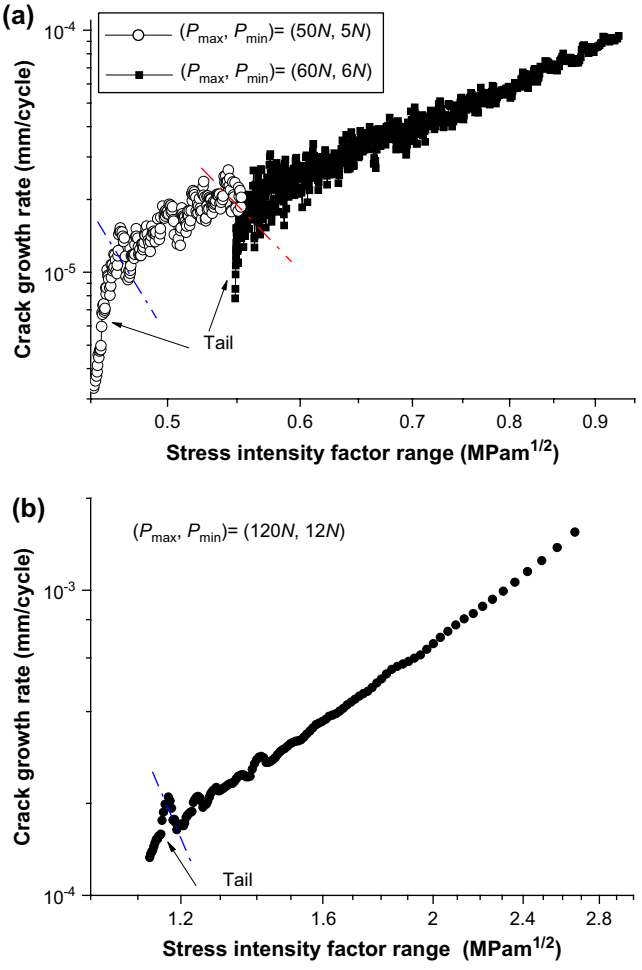

Fig. 6. da/dN–ΔK curves of PC/ABS alloy under different fatigue loadings.

Table 1
Values of C and m for different specimens

Specimen	c1-4	c1-5	c1-6	c1-8	c1-9	c1-10	c1-11	c1-12	c1-13	c1-14
C (10^{-5})	8.8375	9.0398	8.6012	8.6682	11.508	10.194	10.440	11.062	8.8204	9.2886
m	3.0429	2.4877	2.7295	2.8379	2.7498	2.8999	3.0991	2.6103	2.8319	2.9515

Using the (a, N) data pairs, fatigue loading data and seven-point formula deductive technique, a computer program is written to obtain the FCP rate of PC/ABS alloy. Before calculation, E' should be determined according to the crack length calibration. Inputting the value of E', the initial crack length a_0, the dimensions of the specimen, the fatigue load, the crack opening displacement, the number of fatigue cycles, one can then obtain the data (a, N) and (da/dN, ΔK), simultaneously. Also, the curves of a–N and da/dN–ΔK can be obtained.

3. Results and discussions

3.1. Fatigue crack propagation behavior

In this work, extensive fatigue tests for PC/ABS alloy are performed. To obtain the curve of da/dN–ΔK of PC/ABS alloy within a wider range of SIF, the crack growth rate should cover a range of 10^{-6}–10^{-3} mm/cycle and different load ranges are therefore applied to the specimens. Fig. 4 shows an example of the comparison of crack lengths a measured with the improved compliance method and visual microscope method, and an excellent agreement can be seen. It is clear that the improved compliance method has sufficient accuracy in measuring the fatigue crack length, which can greatly reduce testing time and diminish experimental errors.

In what follows, the improved compliance method is employed to measure the a–N curves of PC/ABS alloy under various fatigue loadings. Fig. 5 shows the a–N curves obtained for PC/ABS alloy with some of the fatigue loading cases, i.e. 12–120N, 8–80N and 3.6–36N, respectively. It is clear that the crack growth rate increases rapidly with the increase of fatigue load. The other fatigue loading cases for PC/ABS alloy are 5–50N and 6–60N, which are not plotted here for the purpose of clarity.

Using the a–N data, Eq. (2) and the software mentioned above, the curves of da/dN–ΔK can be easily obtained for PC/ABS alloy. Fig. 6a and b shows the da/dN–ΔK curves of PC/ABS alloy under different loading ranges, corresponding to the different range of SIF. The crack growth is unsteady at smaller range of SIF, as shown in Fig. 6a. The acceleration and deceleration of the crack growth might be consistent with the step crack growth behavior at lower crack growth rate region [10–12]. It is shown in Fig. 6b that the variation of crack growth rate is gradually becoming smaller with the increase of the SIF range.

It is also seen that there are 'tails' in the da/dN–ΔK curves. Similar phenomenon has also been observed in literature [3,5,9]. Although the loading conditions are different for each experiment, the phenomenon is considered as the FCP behaviors in a crack growth inception [9] or near threshold stage [5]. However, as we learned from Fig. 6, the 'tails' appear at the initial stages for the same PC/ABS specimens with identical initial crack lengths, even though the FCP test started at different stress intensity factor ranges. The 'tail' stage is longer when the starting stress intensity factor range is smaller. This means the 'tail' stage cannot be considered as near threshold stage. This is a special phenomenon frequently appearing in the FCP test of polymers. Because the initial crack is introduced by slowly pushing a fresh razor into the specimen, it is natural to consider the plastic zone introduced during the crack initiation process as one of the possible reasons. However, as shown in Fig. 2, because there is no obvious plastic deformation at a fresh crack tip, it is only a minor factor. Other than this, similar 'tail' stages also appear when the specimens are previously fatigue cracked. Further discussion will be given in Section 3.2.

It can be obtained now that the FCP rates in the 'tail' region, which should be a reflection of the transition process of FCP, cannot be considered as normal fatigue crack propagation rates. Removing the crack growth data at the initial 'tail' region, steady crack growth relations for each specimen conform to the Paris relationship. The slope of the curve gives the power m in Eq. (3), and the crack growth rate at ΔK equal to unity defines the factor C. The C and m values can be obtained with the data in the steady crack growth region. Table 1 shows the fitting parameters for each specimen.

By collecting all the FCP data at steady crack growth region of 10 different specimens together, as shown in Fig. 7, the Paris relation for a large range of SIF, i.e. from 0.3 to 3 MPa m$^{1/2}$ is thus obtained. The parameters C and m are

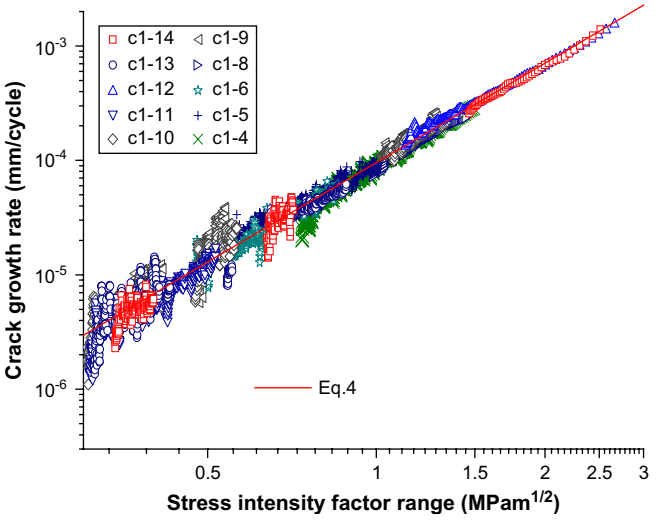

Fig. 7. da/dN–ΔK curve of PC/ABS alloy at steady region of crack propagation. Fatigue loading frequency is 3 Hz, and c1-4 to c1-14 are the marks of specimens.

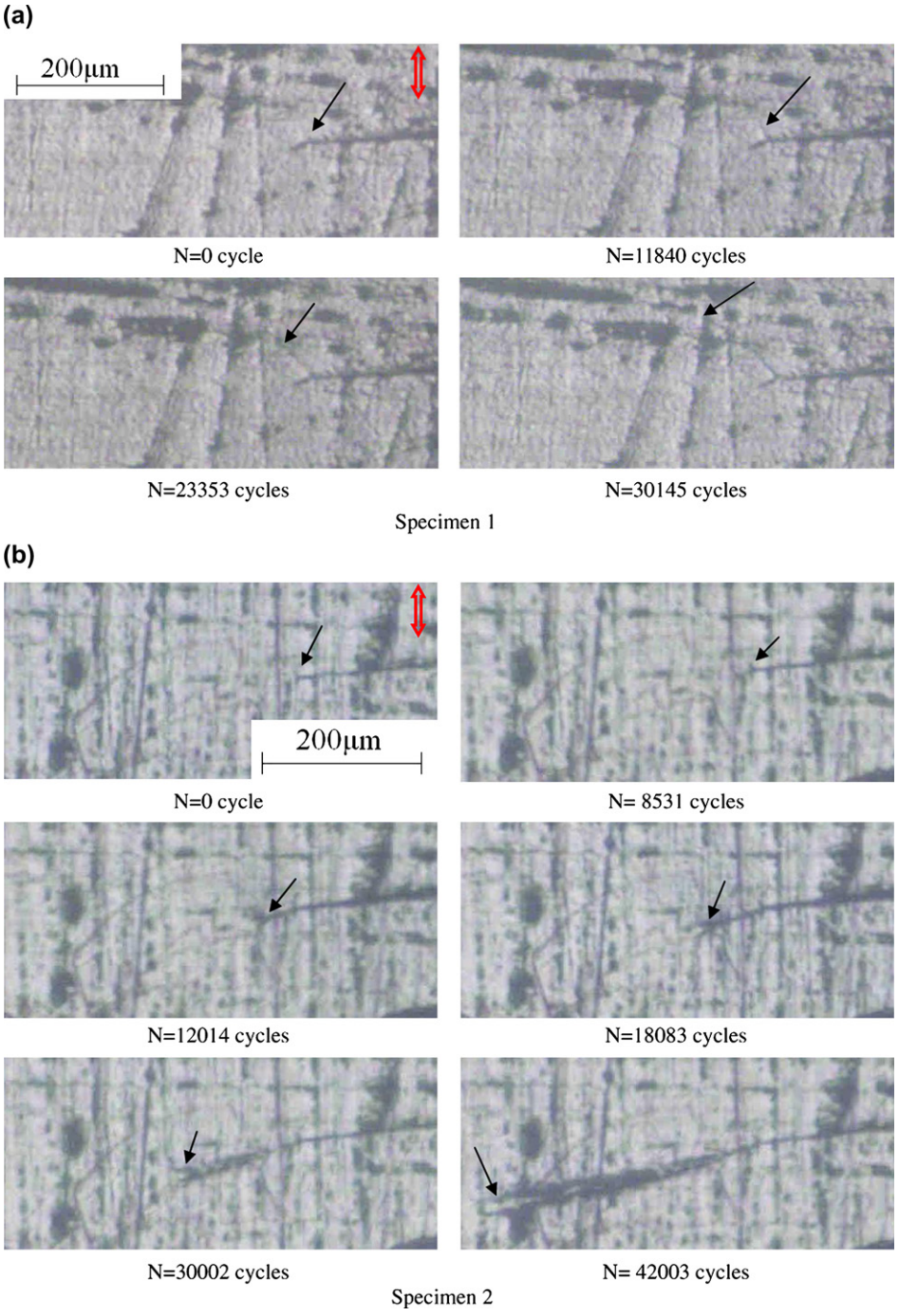

Fig. 8. *In situ* optical observation of crack growth in initial 'tail' stage for two specimens. (The solid and broken arrows show the crack tips and loading direction, respectively.)

9.559×10^{-5} and 2.88 for PC/ABS alloy, respectively. Therefore, the FCP relation can be described as,

$$da/dN = 9.559 \times 10^{-5}(\Delta K)^{2.88} \quad (4)$$

The curve described by Eq. (4) is also plotted in Fig. 7. It is shown that although there is a 'tail' region for each specimen, the FCP relation in steady crack growth region conforms to the Paris crack growth law well.

3.2. Fatigue crack growth in 'tail' stage

To have a clear explanation of the FCP mechanism in the 'tail' stage, close observations of the FCP process in the crack initiation stage are done for all the specimens tested. For most

of the specimens, as shown in Fig. 8a, the crack initiates in a direction of about 40–60° angle with the direction perpendicular to the loading direction. Some cracks initiate in a direction nearly perpendicular to the loading direction, as shown in Fig. 8b. Fig. 9 shows the SEM observation of the crack initiation direction of the specimen shown in Fig. 8a. As we can see from Fig. 8, there are crack growth inception stages for both kinds of specimens. It can be seen from Figs. 8b and 9, that crack growth lines are thin in the previous stage, and thick in the later stage. As we learned from Fig. 9, only little fibrils can be observed on the crack surfaces from point A to point B, while a lot of fibrils appear on the crack surfaces after point B as the crack propagates. The crack growth direction gradually turns to be perpendicular to the tensile loading direction after point B. It has also been observed that crack tip plastic deformation increases with the crack growth in the initiation stage.

It was shown that the FCP in some polymers could be considered as sequential formation and fracture of a craze damage zone [12]. Similarly, there would be a plastic deformation and/or damage accumulation process at crack tip during the 'tail' stage. Cyclic loading can induce large number of tinny cracks near a defect or at crack tip, which leads to the reduction of fracture strain and to the brittleness of polymers [16–19]. The plastic deformation and damage at crack tip would increase as the constant fatigue loading continues in the initiation stage. Fig. 10 shows the state of damage and plastic deformation at the fatigue crack tip during the 'tail' stage simulated with the specimen shown in Fig. 1b after about 2000 fatigue cycles. Comparing with a fresh crack tip shown in Fig. 2b, it can be found that some plastic deformation and microcrazes have been generated at the crack tip during fatigue loading. Because the fatigue loading frequency is low (0.08 Hz), in order to accelerate the test, the fatigue loads in the *in situ* SEM observation test are a little higher than the fatigue loads in the fatigue test on the CT specimen tested in the study, therefore the damage accumulation rate for the eccentric single edge cracked tension specimen is a little higher. Generally, when the damage at crack tip is small, crack might not propagate or only propagate at a very low growth rate during fatigue loading. FCP rate increases with the accumulation of the damage and plastic deformation, and reaches a normal crack growth level when a dynamic balance between the damage accumulation and the crack growth has reached. Then, the normal dynamic balance FCP process would be maintained until the balance is broken by some factors. These can be used to explain the FCP behaviors shown in Fig. 6.

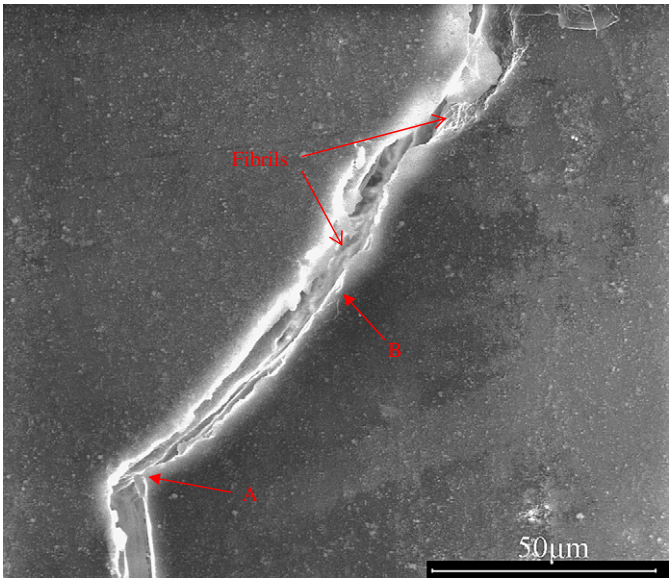

Fig. 9. Close observation of the crack in the initiation stage for the specimen shown in Fig. 8a. (A—pre-crack tip, B—transform point.)

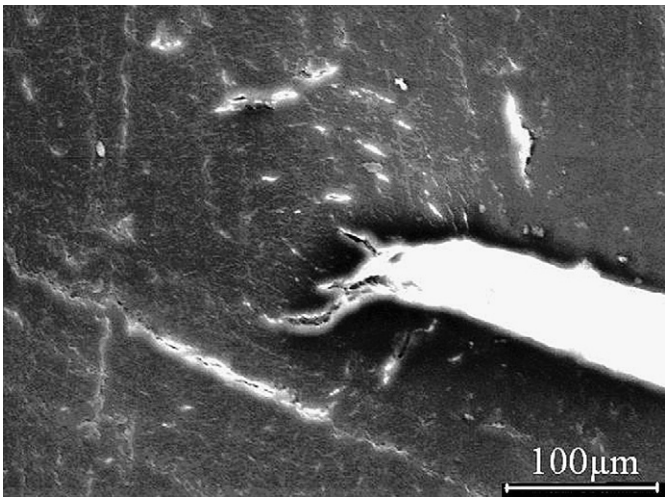

Fig. 10. Fatigue crack tip at 'tail' stage.

3.3. Fractography

To have a better understanding of the FCP mechanism, the fatigue crack surfaces are observed by using SEM. One of the examples of the observed fatigue crack surface pictures of PC/ABS alloy is shown in Fig. 11, in which the features of the regions with different FCP rates are shown. It is clear that the larger the FCP rates, the coarser the fatigue crack surface. In other words, the crack surface becomes coarser with the

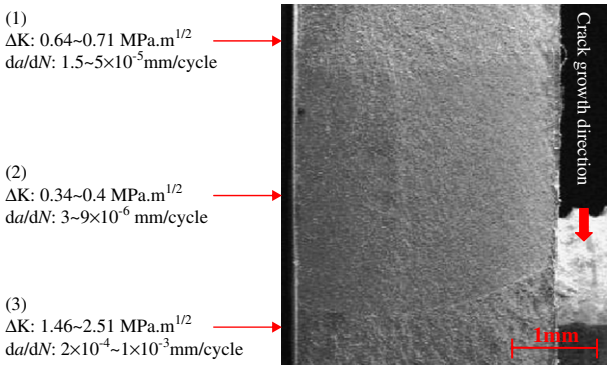

Fig. 11. SEM micrograph of the fatigue fracture surface of PC/ABS alloy. (1) ΔK: 0.64–0.71 MPa.m$^{1/2}$ and da/dN: 1.5–5 × 10^{-5} mm/cycle, (2) ΔK: 0.34–0.4 MPa.m$^{1/2}$ and da/dN: 3–9 × 10^{-6} mm/cycle, and (3) ΔK: 1.46–2.51 MPa.m$^{1/2}$ and da/dN: 2 × 10^{-4}–1 × 10^{-3} mm/cycle.

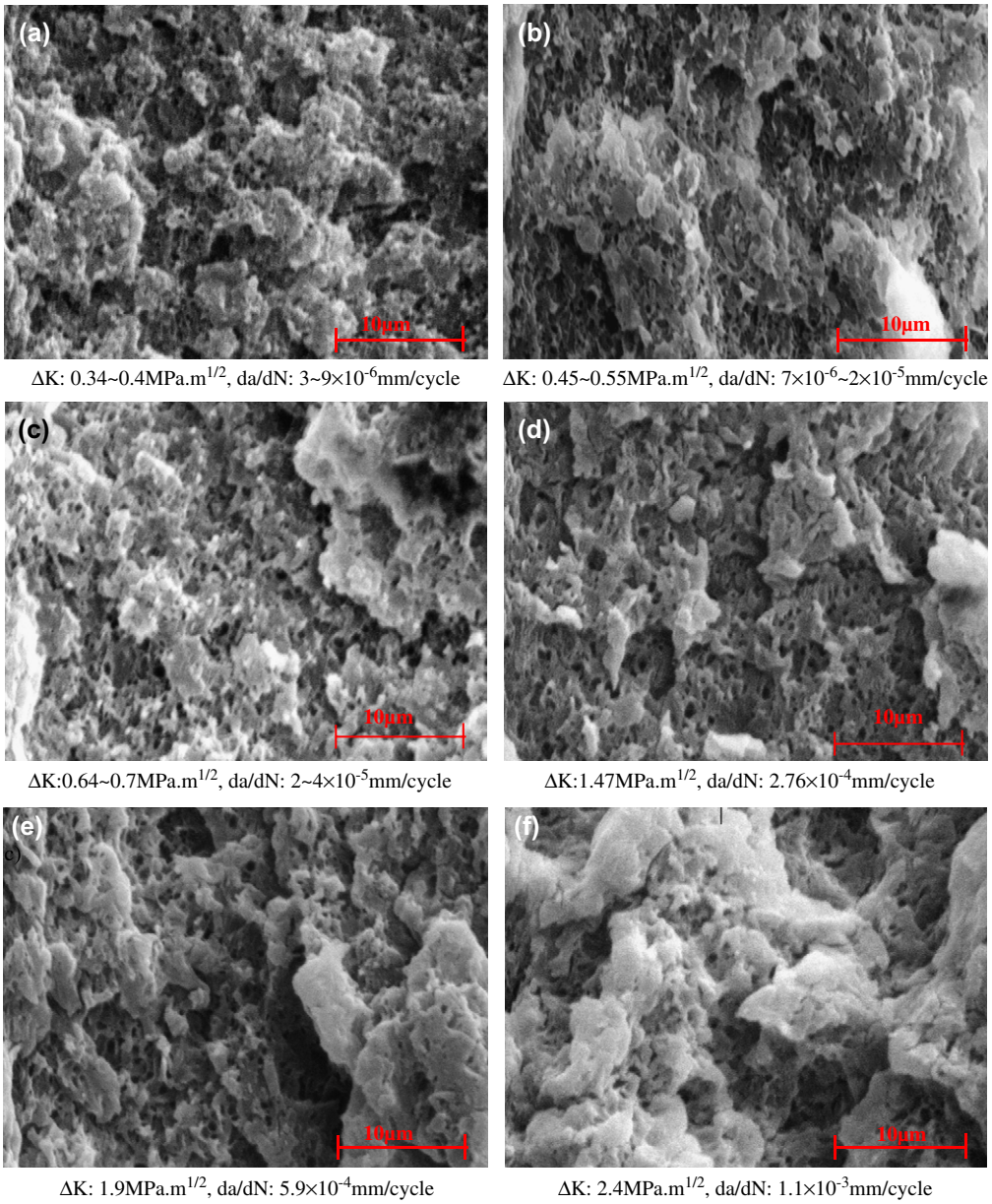

Fig. 12. SEM micrographs of the features of fatigue crack surfaces with different FCP rates for PC/ABS alloy.

increase of the stress intensity factor. Details of the microscopic features of the fracture surface with different crack propagation rates are shown in Fig. 12. It is seen that all the fracture surfaces have microdimple characters, which means that porous structures are being formed near the crack tip during fatigue tests. The larger the stress intensity factors are, the bigger the size of the dimples and the coarser the crack surface. Tear features and second cracks are occasionally observed on the fracture surfaces corresponding to a higher SIF. The fatigue crack propagates through the fracture of the porous structures (or crazes) simultaneously expanding the plastic damage zone near crack tip. Crack tip would have smaller plastic zone and therefore the crack surface becomes smoother if the SIF is small. The chains are stretched out and compressed during fatigue test. More chains are stretched out when larger stress intensity factors are imposed on; therefore the dimple sizes are larger. There is no obvious striation or band feature on the fatigue crack surfaces of the PC/ABS alloy. The crack surfaces near the specimen surfaces are coarser than that in the middle, because the constraint is less near the specimen surface.

As a comparison, Fig. 13 shows us a typical fatigue crack surface for net polycarbonate (PC). It is shown that there are obvious discontinuous crack growth bands (DGBs) on the fatigue crack surface of PC. The dark bands are generated due to the stretching of the polymer chains near the crack tip during the formation of the crack tip craze damage zones, which is restricted to a small area at the crack tip. The bright bands are due to the breaking of the craze damage zones. The DGBs are resulted from the sequential formation and fracture of the crack tip craze zones. Comparing with these two kinds of fatigue crack surfaces shown in Figs. 12 and 13, it can be

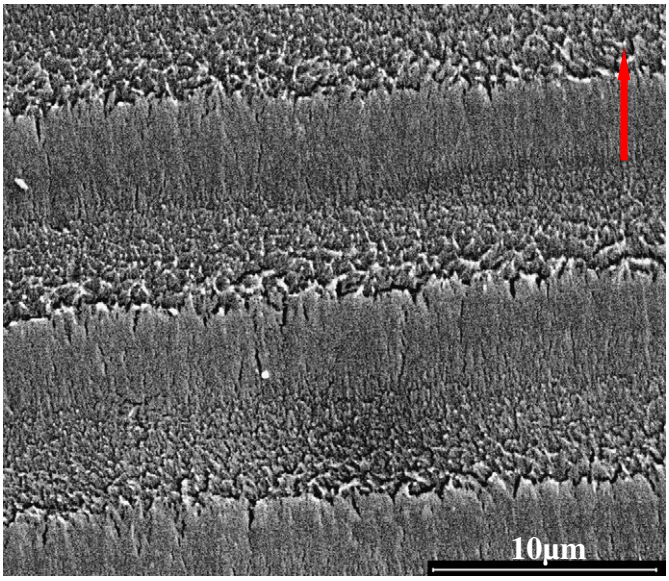

Fig. 13. Typical fatigue crack growth surface for net PC. (The arrow indicates the FCP direction.)

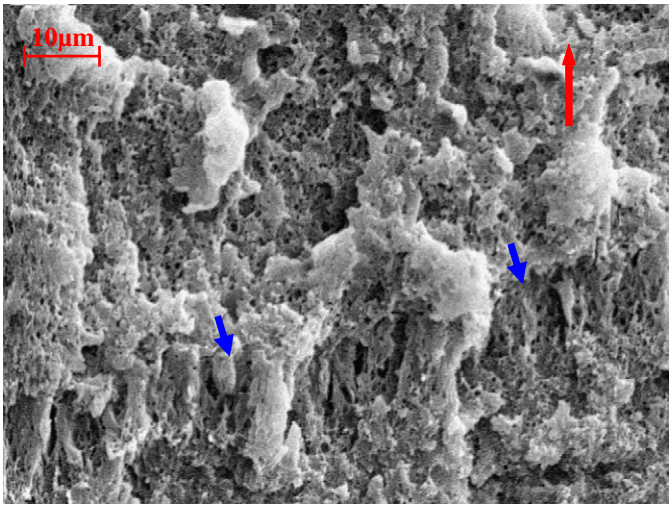

Fig. 15. SEM micrographs of the features of the transformation zone of fatigue crack growth from low (6.12×10^{-6} mm/cycle) to high (2.58×10^{-4} mm/cycle) rate for PC/ABS alloy. The big and small arrows are the crack growth direction and the transformation band.

obtained that the addition of the ABS phase has a great influence on the FCP performance of these materials. This is because the ABS phase can deform more easily than PC. During fatigue loading, as shown in Fig. 14, a lot of crazes are generated around ABS particle-rich regions near a fatigue crack. Therefore, large plastic zones, which can absorb a lot of mechanical energy during fatigue loading, are produced in PC/ABS alloy. These lead to the formation of the dimple structures on the fatigue surface for PC/ABS.

Fig. 15 shows a transformation of crack surface features from low crack growth rate (6.12×10^{-6} mm/cycle) region to high crack growth rate region (2.58×10^{-4} mm/cycle) for PC/ABS alloy. The arrow in the picture shows the crack growth direction. There is a stretched band (like a tension craze zone) between the two crack growth regions. The porous structures in the band are coarser than the fatigue crack surfaces before or after the stretched band. This may be attributed to the action of static loading before the beginning of the higher FCP rate test. However, no similar band is observed when the transformation is from high crack growth rate region to low crack growth rate region. Fig. 16 shows the transformation of crack surface features from high crack growth rate region (4.2×10^{-5} mm/cycle) to low crack growth rate region (4.12×10^{-6} mm/cycle) for PC/ABS alloy. The coarser structures remain for a small range, due to the effects of the higher

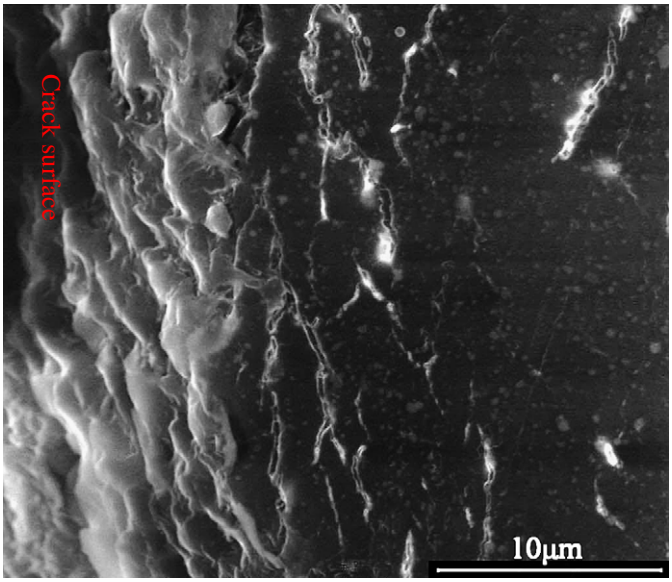

Fig. 14. Crazes generated near ABS particles.

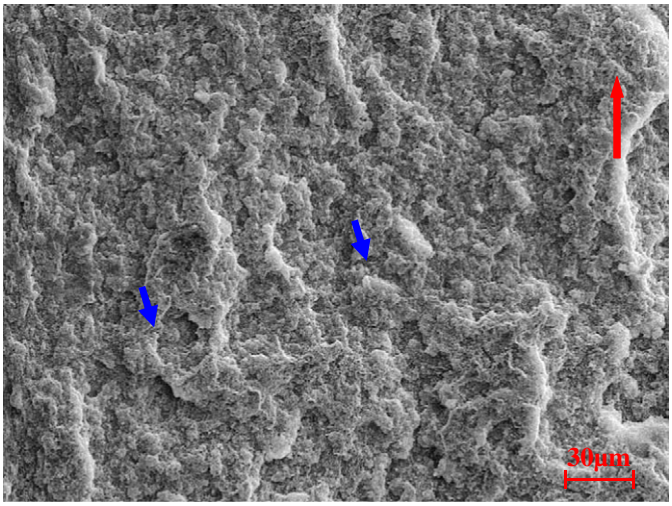

Fig. 16. Microscopic features of the fracture surface in the transformation process of fatigue crack growth from high (4.2E-5 mm/cycle) to low (4.12E-6 mm/cycle) crack growth rates for PC/ABS alloy. The big and small arrows show the crack growth direction and the transformation line, respectively.

stress intensity factor in the higher crack growth rate region. Because the crack initiates in different planes at the beginning of the lower crack growth region, larger energy is needed during the crack growth stage, therefore lower crack growth rate is observed in this region. Gradually the crack surface becomes smoother and the crack growth rate increases to a normal level.

4. Conclusions

The fatigue crack propagation of PC/ABS alloy is experimentally investigated. An improved compliance method is employed to measure the crack propagation of PC/ABS alloy. It is found that there is a 'tail' in the initial FCP stage, which cannot be regarded as FCP threshold stage. The steady FCP relation from low (10^{-6} mm/cycle) to high (10^{-3} mm/cycle) crack growth rate region is obtained for PC/ABS alloy, and it can be described by using the well-known Paris FCP law $da/dN = 9.559 \times 10^{-5}(\Delta K)^{2.88}$. Variation of the FCP rate is larger in lower crack growth rate region than that in higher crack growth rate region.

The addition of ABS into PC has greatly affected the fatigue crack propagation performance of the polymer, which makes the crazes form easily near a crack during fatigue loading. The fractography of fatigue crack surfaces of PC/ABS alloy shows porous and/or dimple features. The coarser structures appear on crack surfaces in the case of higher crack growth rate, and smoother structures appear on the crack surfaces in the case of lower crack growth rate. A stretched band appears on the crack surface when the crack growth transforms from low to high crack growth rates.

Acknowledgements

This work is supported by NSFC (10472087 and 10672129) and 973 Program (2007CB70770). The polymer materials were provided by Nanjing Julong Engineering Plastics Co.

References

[1] Lowe A, Kwon OH, Mai YW. Fatigue and fracture behaviour of novel rubber modified epoxy resins. Polymer 1996;37:565.
[2] Bureau MN, Dickson JI, Denault J. Fatigue propagation behaviour of polystyrene/polyethylene blends. Journal of Materials Science 1998;33:1405.
[3] Bureau MN, Dickson JI, Denault J. Comparison of the fatigue propagation behaviour of polystyrene and 95/5 polystyrene/polyethylene blends. Journal of Materials Science 1998;33:1591.
[4] Niinomi M, Wang L, Enjitsu T, Fukunaga KI. Fatigue characteristics of ultra high molecular weight polyethylene with different molecular weight for implant material. Journal of Materials Science: Materials in Medicine 2001;12:267.
[5] Szabó JS, Gryshchuk O, Karger-Kocsis J. Fatigue crack propagation behavior of interpenetrating vinylester/epoxy resin. Journal of Materials Science Letters 2003;22:1141.
[6] Harcup JP, Duckett RA, Ward IM. Fatigue crack growth in polyethylene: material dependence. I: Tensile/compressive loading. Polymer Engineering and Science 2000;40:627.
[7] Harcup JP, Duckett RA, Ward IM. Fatigue crack growth in polyethylene: material dependence. II: Effects of time "off-load". Polymer Engineering and Science 2000;40:635.
[8] Pruitt L, Bailey L. Factors affecting near-threshold fatigue crack propagation behavior of orthopedic grade ultra high molecular weight polyethylene. Polymer 1998;39:1545.
[9] Baker DA, Hastings RS, Pruitt L. Compression and tension fatigue resistance of medical grade ultra high molecular weight polyethylene: the effect of morphology, sterilization, aging and temperature. Polymer 2000;41:795.
[10] Shah A, Steopanov EV, Hiltner A, Baer E, Klein M. Correlation of fatigue crack propagation in polyethylene pipe specimens of different geometries. International Journal of Fracture 1997;84:159.
[11] Shah A, Steopanov EV, Klein M, Hiltner A, Baer E. Study of polyethylene pipe resins by a fatigue test that simulates crack propagation in a real pipe. Journal of Materials Science 1998;33:3313.
[12] Parsons M, Stepanov EV, Hiltner A, Baer E. Effect of strain rate on stepwise fatigue and creep slow crack growth in high density polyethylene. Journal of Materials Science 2000;35:1857.
[13] Bellinger MA, Sauer JA, Hara M. Fatigue behaviour of sulfonated polystyrene ionomers and their blends with polystyrene. Polymer 1997;38:309.
[14] Li XW, Hristov HA, Yee AF. Influence of cyclic fatigue on the mechanical properties of amorphous polycarbonate. Polymer 1995;36:759.
[15] Ramaswamy S, Lesser AJ. Microscopic damage and macroscopic yield in acrylonitrile–butadiene–styrene (ABS) resins tested under multi-axial stress states. Polymer 2002;43:3743.
[16] Marissen R, Schudy D, Kemp AVJM, Coolen SMH, Duijzings WG, Pol AVD, et al. The effect of material defects on the fatigue behaviour and the fracture strain of ABS. Journal of Materials Science 2001;36:4167.
[17] Wang TJ, Kishimoto K, Notomi M. Effect of triaxial stress constraint on the deformation and fracture of polymers. Acta Mechanica Sinica 2002;18:480.
[18] Favier V, Giroud T, Strijko E, Hiver JM, G'Sell C, Hellinckx S, et al. Slow crack propagation in polyethylene under fatigue at controlled stress intensity. Polymer 2002;43:1375.
[19] Elinck JP, Bauwens JC, Homes G. Fatigue crack growth in poly(vinyl chloride). International Journal of Fracture Mechanics 1971;7:227.
[20] Pulos GC, Knauss WG. Nonsteady crack and craze behavior in PMMA under cyclical loading. International Journal of Fracture 1998;93:145.
[21] Ramsteiner F, Armbrust T. Fatigue crack growth in polymers. Polymer Testing 2001;20:321.
[22] Marissen R, Lange RFM, Biβels S, Hinkel P, Nowack H. Scanning electron microscope visualisation of crack initiation and propagation under static and fatigue loading on thermoplastic elastomers. International Journal of Fatigue 2005;27:71.
[23] Wang TJ, Kishimoto K, Notomi M. A micromechanics criterion for the ductile fracture of a polycarbonate. Key Engineering Materials 2000;183/187:121.
[24] Wildes G, Keskkula H, Paul DR. Fracture characterization of PC/ABS blends: effect of reactive compatibilization, ABS type and rubber concentration. Polymer 1999;40:7089.
[25] Fang QZ, Wang TJ, Li HM. Large tensile deformation behavior of PC/ABS alloy. Polymer 2006;47:5174.
[26] Fang QZ, Wang TJ, Li HM. Investigation on the tensile property of PC/ABS polymer. Key Engineering Materials 2006;326/328:127.
[27] Fang QZ. Fatigue crack growth in steels 42CrV and IR3Mo. Key Engineering Materials 2004;261/263:1179.